

## Single-Doppler Velocity Retrieval with Rapid-Scan Radar Data

ALAN SHAPIRO

*School of Meteorology, and Center for Analysis and Prediction of Storms, University of Oklahoma, Norman, Oklahoma*

PAUL ROBINSON

*Center for Analysis and Prediction of Storms, University of Oklahoma, Norman, Oklahoma*

JOSHUA WURMAN

*School of Meteorology, University of Oklahoma, Norman, Oklahoma*

JIDONG GAO

*Center for Analysis and Prediction of Storms, University of Oklahoma, Norman, Oklahoma*

(Manuscript received 14 February 2003, in final form 19 May 2003)

### ABSTRACT

An approximate (rapid scan) dynamical model for single-Doppler retrieval of the vector wind field is investigated. This approximate model is based on the Lagrangian form of the radial component of the equation of motion and is valid for retrieval time windows that are smaller than the effective timescale of the flow but larger than the product of the effective timescale and (nondimensional) relative error in the radial wind observations. The retrieval was tested with data gathered by two Doppler-on-Wheels mobile Doppler research radars of a cold front on 16 June 2000 near Grandfield, Oklahoma. Experiments focused on the impact of time resolution and the utility of a background constraint obtained from a volume velocity processing (VVP)-like estimate of the wind field. Retrieval error statistics were substantially improved as the volume scan intervals decreased from 5 min [characterizing the current Weather Surveillance Radar-1988 Doppler (WSR-88D) scan rates] down to 1 min. Use of the background constraint also improved the results, with superior results obtained in the high temporal resolution experiments when the background constraint was selectively imposed.

### 1. Introduction

By probing the three-dimensional structure of mesoscale meteorological phenomena such as microbursts, downbursts, tornadic supercells, hailstorms, squall lines, and mesoscale convective systems, Doppler radars have greatly extended our knowledge of these phenomena (Atlas 1990) and enhanced our short-term hazard warning capabilities (Serafin and Wilson 2000). Doppler radar data are also increasingly being used as a data source for hydrologic and numerical weather prediction models, with further societal benefits expected from improved forecasts of floods and hazardous weather (Pereira Fo. et al. 1999; Wilson et al. 1998; Sun and Crook 2001; Weygandt et al. 2002b). Research on the quantitative use of radar data in weather analysis has proceeded on several fronts: (i) quality control to contend with anomalous propagation, ground clutter, radial ve-

locity contamination by bird migrations, and velocity aliasing; (ii) microphysical retrieval to determine type and concentration of hydrometeors; (iii) thermodynamic retrieval to determine pressure, temperature, and humidity fields; and (iv) the analysis of the vector wind field. Although progress has been made in each of these areas, a number of challenges remain. This paper is concerned with the latter problem of wind retrieval.

In regions scanned by two or more Doppler radars, conventional methods of dual-Doppler wind analysis can be used to estimate the wind field from geometric relations, possibly augmented by a statement of mass conservation (e.g., Armijo 1969; Miller and Strauch 1974; Brandes 1977; Ray et al. 1980; Ziegler et al. 1983; Kessinger et al. 1987; Shapiro and Mewes 1999 and references therein). However, even in the United States, where the Weather Surveillance Radar-1988 Doppler (WSR-88D) network provides nearly nationwide data coverage at low and middle levels of the troposphere (Klazura and Imy 1993; Serafin and Wilson 2000; Maddox et al. 2002), the distant spacing between adjacent

---

*Corresponding author address:* Dr. Alan Shapiro, University of Oklahoma, 100 East Boyd, Rm. 1310, Norman, OK 73019.  
E-mail: ashapiro@ou.edu

radars restricts much of the coverage to nonoverlapping data domains from single radars; regions of overlapping radar data coverage are more limited in vertical extent, of coarse spatial resolution, and restricted to relatively high altitudes. New technologies such as bistatic radar networks (Wurman et al. 1993; Wurman 1994) have also been deployed in a few locations, primarily in research applications. Bistatic networks contain passive radar receivers that measure components of the cross-transmit-beam wind. The receivers are inexpensive enough that it is practical to distribute multiple devices over limited areas. Using bistatic data, vector wind fields can be constructed with techniques similar to the dual-Doppler methods referred to above, or with new methods based on variational analysis (Protat and Zawadzki 1999; Gao et al. 1999). Bistatically retrieved vector wind fields have been shown to be accurate, or at least in agreement with standard dual-Doppler calculations (Wurman 1994; Satoh and Wurman 2003; Friedrich and Hagen 2001). However, bistatic networks remain uncommon.

The earliest single-Doppler velocity retrieval methods were based on the assumption that the Cartesian velocity components varied linearly with the spatial coordinates. The parameters in the linear wind models were obtained from a regression analysis as the best fit of the linear wind to the radial velocity data. In the velocity–azimuth display (VAD) analysis pioneered by Probert-Jones (1960), Lhermitte and Atlas (1961), Caton (1963), and Browning and Wexler (1968), the parameters were obtained through a low-order harmonic analysis of data on circles centered on the radar. In the volume velocity processing (VVP) technique of Waldteufel and Corbin (1979) and Koscielny et al. (1982), the parameters were frozen over individual analysis sector volumes. The stability and robustness of the VAD and VVP regressions were explored by Boccippio (1995). Caya and Zawadzki (1992) showed that the parameters of a conventional VAD model could be contaminated by spatial nonlinearities in the wind, and introduced a nonlinear VAD model to mitigate the problem. Caya et al. (2002) extended the conventional VVP framework to include the anelastic mass conservation equation and use of a moving reference frame.

Another early wind retrieval technique, tracking radar echoes by correlation (TREC), estimated the velocity field from the motion of radar echo patterns (Zawadzki 1973; Rinehart 1979; Tuttle and Foote 1990). Echo motion in these studies was obtained by tracking echo centroids or following cross-correlation maxima of features appearing in consecutive radar scans. Since TREC treats reflectivity patterns as passive markers of the flow, it is thought to work best in regions where sedimentation of scatterers and growth or decay of hydrometeors are not occurring, as in the case of the optically clear planetary boundary layer (PBL). However, Smythe and Zrnic (1983) showed that improved horizontal wind retrievals could be obtained in an optically clear PBL dataset when

radial velocity patterns were tracked instead of reflectivity.

Simple techniques that explicitly impose the reflectivity conservation equation have also been developed. Shapiro et al. (1995) used the reflectivity conservation equation and the frozen turbulence approximation to obtain an overdetermined system of two equations for a pseudostreamfunction. A least squares formulation reduced the problem to that of solving a Poisson equation. This method was adapted by Weygandt et al. (2002a) to the retrieval of winds in a supercell thunderstorm. The reflectivity conservation equation was imposed in a moving reference frame in the least squares formulations of Zhang and Gal-Chen (1996), Liou (1999), Lazarus et al. (1999, 2001), and Liou and Luo (2001). Use of a moving reference frame was advocated by Gal-Chen (1982) as a means to reduce discretization errors in temporal derivative terms.

Perhaps the most sophisticated of the wind retrievals are methods that use prognostic equations as strong (exact) or weak (approximate, least squares) constraints in a variational framework with a solution via the local minimization of a cost function (Sasaki 1970a–c). Such methods include the adjoint, least squares, and other four-dimensional variational approaches typically used in data assimilation and parameter estimation. The adjoint retrievals of Sun et al. (1991), Kapitza (1991), and Sun and Crook (1994, 2001) seek the initial conditions of a model (control variables) that minimize a cost function that measures the discrepancies between observed and model-predicted variables over a time window (assimilation window). The wind and thermodynamic variables are simultaneously retrieved using the full equation set of a dry convective numerical model as a strong constraint (necessitating the backward-in-time integration of the corresponding adjoint equations to determine the gradient of the cost function with respect to the control variables). The cost function also includes terms that penalize discrepancies between model-predicted fields and background fields obtained from a forecast or a separate analysis procedure, and terms that impose spatial and temporal smoothness. In principle, the method is flexible enough to retrieve initial conditions, boundary conditions, and parameter values (e.g., mixing coefficients). While the full model adjoint approach is the most sophisticated of the retrieval algorithms, it is computationally intensive as many iterations of the forward and adjoint equations are needed in the search for a cost function minimum. Moreover, the complexity of the problem (initial values of most of the dynamical and thermodynamical variables at all grid points are treated as control variables) may make it susceptible, in some situations, to solution nonuniqueness, that is, the presence of multiple minima in the cost function (Kapitza 1991).

The adjoint method and other variational formulations can also be applied to simpler equations than the full equation set of a numerical convection model. For ex-

ample, the simple adjoint methods of Qiu and Xu (1992) and Xu et al. (1994a,b, 1995, 2001) retrieve the horizontal component of the wind field using the reflectivity conservation equation and/or radial component of the equation of motion as a strong constraint (necessitating the backward integration of the adjoint versions of these simple conservation equations). Provision is made for a time-mean residual forcing term intended to parameterize the effects of processes not explicitly included in the simple prediction model, for example, pressure gradient force in the radial component of the equation of motion. Xu et al. (2001) found that when applying the simple adjoint method to retrieve the horizontal winds in a wet microburst and a gust front, radial velocity conservation is a more appropriate constraint than reflectivity conservation. Laroche and Zawadzki (1994) suggested that when a prognostic equation contained error (as in the reflectivity conservation equation), it was more appropriate to impose it as a weak constraint than a strong constraint. Their retrieval method was the first to include a prognostic equation as a weak constraint. It was also novel in its use of a Lagrangian scheme to integrate the prognostic equation. A key finding was that solution nonuniqueness could be a problem even with an equation as simple as a linear advection equation (and even with mass conservation and smoothness constraints imposed). In a later study, Laroche and Zawadzki (1995) retrieved the steady-state component of the horizontal winds in a clear-air dataset using both reflectivity conservation and radial wind conservation as weak constraints (again, in a Lagrangian framework). Application of a VVP-like constraint (linear wind within sectors) and smoothness constraint improved the results. Qiu and Xu (1996) compared the simple-adjoint algorithm with a least squares algorithm that imposed the radial component of the equation of motion as a weak constraint. When weak constraints on divergence and vorticity were imposed for smoothness, the simple adjoint and least squares retrievals produced comparable results.

Gao et al. (2001) extended the simple adjoint framework to three dimensions and included the anelastic mass conservation equation as a weak constraint. Tests with simulated supercell data were performed with the radial component of the equation of motion imposed as a strong constraint (requiring the adjoint of that equation) with provision for a time-mean residual forcing term. Xu et al. (2001) also extended the simple adjoint framework to three dimensions and included the incompressibility condition. In this latter study both reflectivity conservation and the radial component of the equations of motion were imposed as strong constraints (requiring adjoints of these equations). The three component equations of motion and the divergence equation obtained from the divergence of the equations of motion were also imposed, but as weak constraints so as to avoid the introduction of additional adjoint equations. Because this retrieval made explicit provision for buoy-

ancy and pressure gradient forces in the weak dynamical constraints, it was also possible to explicitly include the radial component of the pressure gradient and buoyancy forces in the radial component equation of motion [in contrast to parameterizing these effects in a residual forcing term as in Gao et al. (2001)]. Smoothness was enforced by using spline basis function representations of the model variables and their time tendencies.

Many of the simpler (non-full-model-adjoint) wind retrieval algorithms made explicit or implicit use of a temporal constraint such as velocity stationarity, Taylor's frozen turbulence hypothesis, or the retention of only the time-mean part of the wind and forcing terms. Since the validity of these constraints degrades with increasing duration of a time window, one might expect a decrease in retrieval skill with decreased temporal resolution of the observations. Qiu and Xu (1996) report a reduction in the error of microburst winds in two retrieval methods when the scan period was decreased from the 5 min representative of WSR-88D radars to the 60 s of a terminal Doppler weather radar (TDWR). Similarly, Lazarus et al. (1999) showed that errors in the Gal-Chen-Zhang retrieval could be substantially reduced by reducing the scan period. However, in general, one might expect a limit on how small a scan period should be before noise would overwhelm the retrieval. Moreover, it is not clear that small scan periods would be beneficial at far ranges, where the spatial resolution becomes large.

In this study we explore the utility of rapid-scan radar data in a simple single-Doppler velocity retrieval algorithm. The algorithm combines aspects of the Xu et al. (1994b, 1995) and Gao et al. (2001) simple adjoint retrievals with the Laroche and Zawadzki (1994, 1995) Lagrangian variational retrievals. We adopt the Lagrangian framework because it is conceptually and computationally simple, permits analytic solution of the dynamical model, and facilitates visualization of the cost function. As in the Xu et al. and Gao et al. studies, we impose the radial component of the equation of motion as a strong constraint, but with a bulk forcing term treated as an additional control variable (along with the initial cross-beam velocity components). As in Laroche and Zawadzki (1995), the control variables are frozen over a sector or "patch" of parcels rather than over just one parcel in order to stabilize the estimates of the control variables (in essence, the patch allows us to take advantage of high temporal resolution by sacrificing spatial resolution). Provision is also made for a background azimuthal wind constraint in which the background wind vectors are obtained from a piecewise linear wind model (as in VVP). In some of our experiments the background constraint was only imposed in regions where the deviation of the observed radial wind from the radial component of the background wind was less than a threshold value. Although most of the aspects of this retrieval are variations on previous work, the derivation of the approximate (rapid scan) dynamical model

is new and leads to fundamental inequalities for the acceptable duration of the retrieval time window that should be applicable to many of the simple retrieval methods. The upper bound inequality provides a dynamical definition of “rapid scan.” The selective manner in which the background constraint is imposed is also new and may be broadly applicable to all the retrieval methods.

The retrieval is tested with data gathered by two Doppler-on-Wheels (DOWs) pulsed X-band mobile Doppler radars of a cold front on 16 June 2000 near Grandfield, Oklahoma. These research radars have full scanning capability, real-time displays and archiving, and are mounted on trucks for easy portability (Wurman et al. 1997; Wurman 2001). Radial velocity data from one DOW are supplied to the retrieval, while radial velocity data from both DOWs are supplied to a dual-Doppler wind analysis that is used to verify the retrieved azimuthal wind component. Experiments focused on the impact of time resolution, the utility of a selectively imposed background constraint, and the sensitivity to patch size.

The plan of the paper is as follows. In section 2 we derive an approximate dynamical model appropriate for small retrieval time windows, and obtain the main theoretical results for this study: two flow-dependent inequalities that quantify the appropriate duration of the retrieval time windows for the rapid-scan model. The estimation of the VVP-like background winds are described in section 3. Section 4 describes how the retrieval combines the rapid-scan dynamical model and background field information. The retrieval is tested with the cold front data in section 5. The main findings are summarized in section 6.

## 2. A dynamical model for rapid-scan single-Doppler velocity retrieval

### a. Exact dynamical model

It will be convenient to work with both a Cartesian  $(x, y, z)$  coordinate system centered on the radar and a “radar coordinate system,” a spherical polar  $(r, \phi, \theta)$  coordinate system centered on the radar (Fig. 1). Here we follow the standard meteorological convention that the  $x$  axis points toward the east, the  $y$  axis points toward the north, the azimuthal angle  $\phi$  is reckoned clockwise from the north, and the polar (elevation) angle  $\theta$  is measured upward from the horizontal plane. The radial velocity component,  $u_r \equiv dr/dt$ , is measured by the Doppler radar. The azimuthal velocity component,  $u_\phi \equiv r \cos\theta \, d\phi/dt$ , and the polar velocity component,  $u_\theta \equiv r \, d\theta/dt$ , are the cross-beam wind components we seek to retrieve.

In Cartesian coordinates, the Lagrangian form of the equations of motion for an air parcel can be written as

$$\frac{du}{dt} = a, \quad \frac{dv}{dt} = b, \quad \frac{dw}{dt} = c, \quad (1)$$

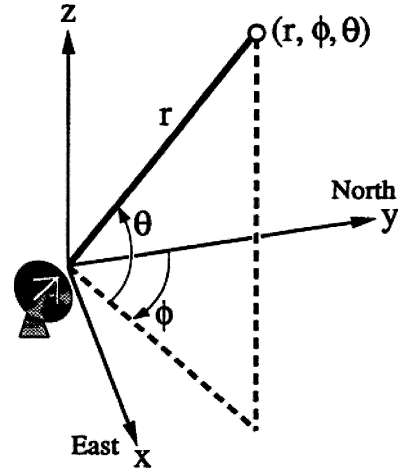


FIG. 1. Spherical polar coordinate system  $(r, \phi, \theta)$  with radar at the origin. The local vertical through the origin is specified by  $\theta = \pi/2$ , and the northerly azimuth angle is given by  $\phi = 0$ . Azimuthal angle  $\phi$  increases in the clockwise direction.

where  $u \equiv dx/dt$ ,  $v \equiv dy/dt$ , and  $w \equiv dz/dt$  are the Cartesian velocity components; and  $a$ ,  $b$ , and  $c$  are the net forces per unit mass exerted on the air parcel. These forces are, in general, time dependent, and can be expressed in a Taylor series as

$$a = \sum_{n=0}^{\infty} a_n \frac{t^n}{n!}, \quad b = \sum_{n=0}^{\infty} b_n \frac{t^n}{n!}, \quad c = \sum_{n=0}^{\infty} c_n \frac{t^n}{n!}, \quad (2)$$

where

$$a_n \equiv \left. \frac{d^n a}{dt^n} \right|_{t=0}, \quad b_n \equiv \left. \frac{d^n b}{dt^n} \right|_{t=0}, \quad c_n \equiv \left. \frac{d^n c}{dt^n} \right|_{t=0}. \quad (3)$$

Applying (2) in (1), and integrating with respect to time, we obtain the velocity components as

$$\begin{aligned} u &= u_0 + a_0 t + O(t^2), \\ v &= v_0 + b_0 t + O(t^2), \\ w &= w_0 + c_0 t + O(t^2), \end{aligned} \quad (4)$$

where  $u_0$ ,  $v_0$ , and  $w_0$  are the initial values of  $u$ ,  $v$ , and  $w$ , respectively, and  $O$  is a mathematical order symbol (Kundu and Cohen 2002). The time derivatives of the force components appear in second- and higher-order terms in (4).

Integrating (4) with respect to time yields

$$\begin{aligned} x &= x_0 + u_0 t + \frac{a_0}{2} t^2 + O(t^3), \\ y &= y_0 + v_0 t + \frac{b_0}{2} t^2 + O(t^3), \quad \text{and} \\ z &= z_0 + w_0 t + \frac{c_0}{2} t^2 + O(t^3), \end{aligned} \quad (5)$$

where  $x_0$ ,  $y_0$ , and  $z_0$  are the initial values of  $x$ ,  $y$ , and

$z$ , respectively. Applying (5) in  $r^2 = x^2 + y^2 + z^2$ , we obtain the radial coordinate of the parcel as

$$\begin{aligned} r^2 &= x_0^2 + y_0^2 + z_0^2 + 2(x_0u_0 + y_0v_0 + z_0w_0)t \\ &+ (u_0^2 + v_0^2 + w_0^2 + a_0x_0 + b_0y_0 + c_0z_0)t^2 \\ &+ (a_0u_0 + b_0v_0 + c_0w_0)t^3 \\ &+ \frac{1}{4}(a_0^2 + b_0^2 + c_0^2)t^4 + O(t^5). \end{aligned} \quad (6)$$

It is convenient to rewrite the zeroth-, first-, and second-order terms on the right-hand side of (6) in spherical polar coordinates:  $x_0^2 + y_0^2 + z_0^2 = r_0^2$ ,  $x_0u_0 + y_0v_0 + z_0w_0 = \mathbf{r}_0 \cdot \mathbf{u}_0 = r_0u_{r_0}$ ,  $u_0^2 + v_0^2 + w_0^2 = u_{\phi_0}^2 + u_{\theta_0}^2$ , and  $a_0x_0 + b_0y_0 + c_0z_0 = \mathbf{r}_0 \cdot \mathbf{f}_0 = r_0a_{r_0}$ , where  $\mathbf{f}_0 \equiv a_0\hat{i} + b_0\hat{j} + c_0\hat{k}$  is the initial force vector and  $a_{r_0} \equiv \hat{\mathbf{r}} \cdot \mathbf{f}_0$  is the initial radial component of the force. Equation (6) then becomes

$$\begin{aligned} r^2 &= r_0^2 + 2r_0u_{r_0}t + (u_{r_0}^2 + u_{\phi_0}^2 + u_{\theta_0}^2 + a_{r_0}r_0)t^2 \\ &+ (a_0u_0 + b_0v_0 + c_0w_0)t^3 \\ &+ \frac{1}{4}(a_0^2 + b_0^2 + c_0^2)t^4 + O(t^5). \end{aligned} \quad (7)$$

Taking the time derivative of (7) and using  $u_r = dr/dt$ , we obtain the radial velocity of the parcel as

$$\begin{aligned} ru_r &= r_0u_{r_0} + (u_{r_0}^2 + u_{\phi_0}^2 + u_{\theta_0}^2 + a_{r_0}r_0)t \\ &+ \frac{3}{2}(a_0u_0 + b_0v_0 + c_0w_0)t^2 \\ &+ \frac{1}{2}(a_0^2 + b_0^2 + c_0^2)t^3 + O(t^4). \end{aligned} \quad (8)$$

To obtain an expression for the azimuthal coordinate of the parcel, apply  $u_\phi = r \cos\theta \, d\phi/dt$  in the Taylor expansion  $\phi = \phi_0 + d\phi/dt|_{t=0}t + d^2\phi/dt^2|_{t=0}t^2/2 + O(t^3)$ :

$$\phi = \phi_0 + \frac{u_{\phi_0}}{r_0 \cos\theta_0}t + \frac{d}{dt}\left(\frac{u_\phi}{r \cos\theta}\right)\bigg|_{t=0} \frac{t^2}{2} + O(t^3). \quad (9)$$

Similarly, by applying  $u_\theta = r d\theta/dt$  in the Taylor expansion  $\theta = \theta_0 + d\theta/dt|_{t=0}t + d^2\theta/dt^2|_{t=0}t^2/2 + O(t^3)$ , we obtain the elevation angle of the parcel as

$$\theta = \theta_0 + \frac{u_{\theta_0}}{r_0}t + \frac{d}{dt}\left(\frac{u_\theta}{r}\right)\bigg|_{t=0} \frac{t^2}{2} + O(t^3). \quad (10)$$

Thus, Newton's second law has yielded a prediction model (8) for a parcel's radial velocity component and formulas (7), (9), and (10) for the parcel trajectory.

#### b. Approximate (rapid scan) dynamical model

Since no assumptions or approximations were made in the derivation of (7)–(10) other than the ordinary continuity restriction in the Taylor expansions, this sys-

tem contains an infinite number of degrees of freedom. We could, in principle, truncate this system after a large but finite number of terms, and use the truncated equations as the basis of a retrieval algorithm (if computational resources permitted). However, such a relatively complete prediction system is not necessarily the most suitable for retrieval purposes. The parameter retrieval problem in a variational framework generally involves the minimization of a cost function with respect to a number of control variables (the variables we wish to retrieve). As the number of degrees of freedom increases, so does the threat of solution nonuniqueness. The most appropriate retrieval algorithm may involve a compromise whereby the prediction model contains enough degrees of freedom to capture the essential physics of the phenomenon being modeled, but not so many degrees of freedom that nonuniqueness becomes a problem. As demonstrated by Li (1991), the number of cost function minima may also depend on the length of the assimilation window. We also note that the threat of nonuniqueness may be less of an issue in retrievals or data assimilation procedures that use numerical weather prediction model forecast fields as background constraints than in "pure" retrievals where numerical weather prediction model forecast fields are not used. If the dynamical constraints alone were subject to severe nonuniqueness, the addition of a background constraint would be expected to guide a solution close to that representing the background state. In such a case the background constraint would mitigate the problem of nonuniqueness, but the quality of the solution would be tied to that of the background state.

We now explore the legitimacy of neglecting the higher-order terms in this system, starting with the terms in the radial velocity formula (8). The lowest-order appearance of any of the force components in (8) is the initial radial force component,  $a_{r_0}$ , which appears in the first-order term. The initial force components in all three directions and the time derivatives of the force components appear in the second- or higher-order terms. These terms will be negligible if the retrieval extends over a small enough time window. The condition for the safe neglect of these terms is

$$|a_0u_0 + b_0v_0 + c_0w_0|t^2 \ll |u_{r_0}^2 + u_{\phi_0}^2 + u_{\theta_0}^2 + a_{r_0}r_0|t, \quad \text{or} \quad AUt \ll \max(U^2, Ar_0), \quad (11)$$

where  $U$  is a characteristic velocity scale and  $A$  is a characteristic acceleration scale.

Error considerations lead to a second inequality of the opposite sense. To ensure that errors in the zeroth-order term in (8) are much smaller than the first-order term itself, we must have  $\varepsilon r_0 \ll$

$$|u_{r_0}^2 + u_{\phi_0}^2 + u_{\theta_0}^2 + a_{r_0}r_0|t, \quad \text{or} \quad \varepsilon r_0 \ll t \max(U^2, Ar_0), \quad (12)$$

where  $\varepsilon$  is a measure of the typical observational and analysis errors. Observational errors can be due to in-

strument error, ground clutter and other sidelobe contamination, velocity folding, second-trip echoes, anomalous propagation, and signal contamination by birds. Analysis errors include interpolation errors and errors in the representativeness of the data.

Combining the inequalities (11) and (12), we get

$$\frac{\varepsilon r_0}{\max(U^2, Ar_0)} \ll t \ll \max\left(\frac{U}{A}, \frac{r_0}{U}\right). \quad (13)$$

Scaling the acceleration as

$$A = \max(U/T, U^2/L), \quad (14)$$

where  $L$  is a characteristic length scale and  $T$  is a characteristic timescale, and using the fact that  $1/\max(a, b) = \min(1/a, 1/b)$ , (13) becomes

$$\frac{\varepsilon}{U} \min\left(T, \frac{L}{U}, \frac{r_0}{U}\right) \ll t \ll \max\left[\min\left(T, \frac{L}{U}, \frac{r_0}{U}\right)\right]. \quad (15)$$

Turning now to the azimuthal and polar components of the trajectory, we see that the second- (and higher-) order terms in (9) and (10) will be much smaller than the corresponding first-order terms for times small enough that  $\max(A/r_0, U^2/r_0^2)t^2 \ll (U/r_0)t$ , or, in view of (14),

$$t \ll \min\left(T, \frac{L}{U}, \frac{r_0}{U}\right). \quad (16)$$

As part of this derivation we assumed that a term  $(U^2/r_0^2) \tan\theta_0$  arising from (9) was smaller than  $U^2/r_0^2$ , and could be neglected. This is a valid assumption as long as we restrict our attention to elevation angles smaller than  $45^\circ$ .

The inequality (16) is more restrictive (and therefore supersedes) the inequality on the right-hand side of (15). Amending (15), we obtain

$$\frac{\varepsilon}{U} \min\left(T, \frac{L}{U}, \frac{r_0}{U}\right) \ll t \ll \min\left(T, \frac{L}{U}, \frac{r_0}{U}\right). \quad (17)$$

The inequality (16) [last part of (17)] is a dynamical ‘‘rapid-scan condition’’ that must be met if higher-order terms in the trajectory and radial velocity formulas are to be safely neglected. The rapid-scan condition is that  $t$  must be much smaller than an effective timescale, which is the smallest of (i) the intrinsic timescale  $T$  for an evolving flow, (ii) the advection time  $L/U$  for a parcel moving at speed  $U$  to traverse a distance  $L$ , and (iii) the advection time  $r_0/U$  for a parcel moving at speed  $U$  to traverse a distance  $r_0$ . Thus, rapid-scan data can be expected to be most helpful in conditions of rapid flow evolution (e.g., microbursts, rapidly evolving convective storms) or in flows characterized by small length scales (e.g., narrow fronts, wind shift lines, boundary layer rolls) or in regions close to the radar. Clearly there are numerous scenarios where the time window should

be much shorter than 5 min, the fastest operational scanning period of the WSR-88Ds.

However, the first part of (17) shows that the acceptable length of a retrieval time window must be large enough to compensate for the effects of error in the data. If we assume that  $\varepsilon$  is 10% of  $U$  and consider a rapidly evolving flow with a 3-min timescale [assumed to be smaller than the two advection timescales in (17)], then (17) states that  $t$  should be much larger than 18 s and much smaller than 3 min. On the other hand, if we consider a slowly evolving flow with large advection timescales (e.g., a nearly uniform flow with large radius of curvature far from the radar), then  $t$  will need to be substantially larger. For a flow with an intrinsic 30-min timescale and equivalently large advection timescales (and again assuming  $\varepsilon = 0.1 U$ ),  $t$  will need to be much larger than 3 min. The inequalities in (17) suggest that the appropriate duration of a retrieval time window in the rapid-scan model is flow dependent and may vary substantially throughout the domain. Moreover, if errors in the data are large enough, the rapid-scan model will not be valid for any time window. Although this rapid-scan condition was derived for our particular retrieval technique, it should be generally applicable to any variational retrieval technique that uses a simplified or quasi-steady equation of motion (e.g., Laroche and Zawadzki 1995; Qiu and Xu 1996; Gao et al. 2001; Xu et al. 2001).

If (17) is satisfied, then the dynamical model (7)–(10) can be safely approximated by the rapid-scan model:

$$r(t) = [r_0^2 + 2r_0u_{r0}t + (u_{r0}^2 + u_{\phi0}^2 + u_{\theta0}^2 + a_{r0}r_0)t^2]^{1/2}, \quad (18)$$

$$\phi(t) = \phi_0 + \left(\frac{u_{\phi0}}{r_0 \cos\theta_0}\right)t, \quad (19)$$

$$\theta(t) = \theta_0 + \left(\frac{u_{\theta0}}{r_0}\right)t, \quad (20)$$

$$u_r(t) = \frac{1}{r(t)}[r_0u_{r0} + (u_{r0}^2 + u_{\phi0}^2 + u_{\theta0}^2 + a_{r0}r_0)t]. \quad (21)$$

It is shown in the appendix that (21) is just the discretized Lagrangian form of the radial component of the equation of motion with forcing terms evaluated at the initial time.

This rapid-scan model has just three degrees of freedom per parcel: the initial azimuthal velocity component  $u_{\phi0}$ , initial polar velocity component  $u_{\theta0}$ , and initial radial force component  $a_{r0}$ . The model does not restrict the time to be a positive quantity so it is equally valid for trajectories running forward or backward in time.

### 3. VVP-like estimate of background winds

Background winds obtained from single-Doppler radial velocity data will be used as an additional constraint in the retrieval. In this section we describe the construc-

tion of these background winds and discuss an objective measure of the local “trustworthiness” of these winds that will be used in the experiments where the background constraint is selectively imposed. The background wind estimation is a simple variant of the volume velocity processing (VVP) technique described in the introduction.

Background winds are estimated at each analysis point from radial velocity data within a small squarelike area or “patch” centered at that point. Each background patch subtends  $30^\circ$  in azimuth and extends across an equivalent physical distance in the radial direction. Accordingly, the patches expand with radius. Since each analysis point is associated with its own background

patch, we consider a succession of overlapping patches. The background winds within each patch are considered to be uniform in the horizontal but linearly varying in height:

$$u = U + U'(z - z_0), \quad v = V + V'(z - z_0). \quad (22)$$

Here  $z_0$  is the height of the analysis point (height of the center of the patch),  $U$  and  $V$  are the horizontally uniform background wind components, and  $U'$  and  $V'$  are the constant vertical shear components. Since the patch is on a conical surface (constant elevation angle),  $z$  varies slowly throughout the patch. To estimate  $U$ ,  $V$ ,  $U'$ , and  $V'$  for each patch, apply (22) in the approximate (low-elevation angle) geometrical relation  $u_r = xu/r + yv/r$  and define the mean-squared error in this equation as

$$Q = \frac{\sum \Delta v \left\{ u_r - \frac{x}{r}[U + U'(z - z_0)] - \frac{y}{r}[V + V'(z - z_0)] \right\}^2}{\sum \Delta v}, \quad (23)$$

where  $\Delta v \equiv r^2 \cos \theta \Delta r \Delta \theta \Delta \phi$  is a differential volume element and the sums extend across all the data in the patch. With radial wind observations used in (23),  $Q$  is the mean-squared error in the radial component of the background winds. We seek values of  $U$ ,  $V$ ,  $U'$ , and  $V'$  that minimize this error. Accordingly, we consider  $\partial Q/\partial U = 0$ ,  $\partial Q/\partial V = 0$ ,  $\partial Q/\partial U' = 0$ , and  $\partial Q/\partial V' = 0$ . The resulting set of four linear algebraic equations are readily solved analytically using Cramer’s rule.

Once the background winds have been obtained by this procedure, we substitute them back into (23) to obtain the error in the radial component of the background winds. We hypothesize that the value of  $Q$  can be used as a crude measure of the trustworthiness of the background winds. In regions where  $Q$  is large, we anticipate that the background winds will contain large errors. In some of our retrieval experiments, a background wind constraint will be selectively imposed: in regions where  $Q$  is less than a threshold value, we use the azimuthal component of the retrieved VVP-like winds as a background constraint; in regions where  $Q$  exceeds the threshold, we do not impose any background constraint. The results presented in section 5 are for a threshold value of  $Q = 0.5$ . This method of obtaining the background winds and of flagging regions of trustworthiness has been tested with several datasets, with encouraging results. However, because there is no rigorous justification for why low values of error in the radial component of the background winds should generally be correlated with low values of error in the tangential component of the background winds, we will give very low relative weight to the background winds (relative to the dynamical constraint), even in regions where we “trust” them.

#### 4. Retrieval algorithm

The retrieval is composed of a dynamical prediction model and a background wind constraint. The dynamical model is the set of approximate (rapid scan) equations derived in section 2b, and the background wind model is the linear VVP-like model described in section 3b. The dynamical model is imposed as a strong constraint, as in the simple adjoint approach (e.g., Gao et al. 2001). Following Laroche and Zawadzki (1995), we freeze the values of the control variables (in our case  $u_{\phi_0}$ ,  $u_{\theta_0}$ , and  $a_{r_0}$ ) within small squarelike areas or patches of points on the conical ( $r$ ,  $\phi$ ) surface centered on each analysis point. Each patch subtends a fixed increment of azimuthal angle and has a radial thickness equal to its physical azimuthal length. These retrieval patches need not be the same size as the patches used in the background wind calculation. Use of the patch (ensemble of trajectories) is found to stabilize the estimates of the control variables and reduce noise in the retrieval. Use of the patch may improve accuracy by reducing the effective value of  $\varepsilon$  in the inequality (17).

For each analysis point we seek the values of  $u_{\phi_0}$ ,  $u_{\theta_0}$ , and  $a_{r_0}$  that yield the best agreement between the observed and dynamically predicted values of  $u_r$  along the ensemble of air parcel trajectories originating within the corresponding patch, subject (in some locations) to an azimuthal background wind constraint. Each air parcel within the ensemble is initially ( $t = 0$ ) collocated with an analysis point; that is, the trajectories run forward or backward in time from analysis points.

Accordingly, we seek to minimize the cost function:

$$J = J_1 + \mu J_2, \quad (24)$$

where  $J_1$  is a measure of the error in the predicted radial velocity component,  $J_2$  is a measure of the discrepancy between  $u_{\phi 0}$  and the azimuthal component of the background wind, and  $\mu$  is a relative weight coefficient. Note that  $J_1$  (and therefore  $J$ ) is a function of  $u_{\phi 0}$ ,  $u_{\theta 0}$ , and  $a_{r0}$ , while  $J_2$  is just a function of  $u_{\phi 0}$ .

The dynamical cost function  $J_1$  is defined by

$$J_1 \equiv \sum_{k=1}^K \sum_{m=1}^M W_m \Delta_{m,k}^2, \quad (25)$$

where  $m$  is a time index,  $k$  is a parcel index,  $M$  is the number of time levels used in the retrieval,  $K$  is the number of parcels in the patch surrounding each analysis point,  $\Delta_{m,k}$  is the discrepancy at time  $t_m$  between the  $k$ th parcel's predicted radial velocity and the observed radial velocity interpolated (trilinearly) to the parcel location, and  $W_m \sim |1/t_m|$  is a time-dependent weighting function. The radial velocity prediction is given by (21), with the trajectory calculated from (18)–(20).

The background cost function  $J_2$  penalizes azimuthal winds that depart from background azimuthal winds:

$$J_2 \equiv \sum_{k=1}^K \sum_{m=1}^M W_m \delta_k^2. \quad (26)$$

Here  $m$ ,  $k$ ,  $M$ ,  $K$ , and  $W_m$  are defined as above, and  $\delta_k$  is the discrepancy between the initial azimuthal velocity component  $u_{\phi 0}$  and the projection of the background wind vector in the azimuthal direction; that is,  $\delta_k \equiv u_{\phi 0} - (\mathbf{U}\mathbf{i} + \mathbf{V}\mathbf{j}) \cdot \boldsymbol{\varphi}$ , where  $\mathbf{i}$ ,  $\mathbf{j}$ , and  $\boldsymbol{\varphi}$  are the unit vectors in the east, north, and azimuthal directions, respectively. It can be noted that even though the calculation of  $U$  and  $V$  was based on an assumed horizontal uniformity of background winds within each background patch, the successive calculation of  $U$  and  $V$  on overlapping patches yields values that vary slowly in the horizontal.

The weighting function  $W_m \sim |1/t_m|$  was constructed to give lesser weight to observations far from the initial (retrieval) time. This was deemed desirable because the validity of the rapid-scan model degrades with time. However, it should be noted that in the two-time-level experiments presented in the next section (which form the majority of the presented experiments), the retrieval results are independent of the weighting function. This is because in the two-time-level experiments, one time level corresponds to the initial (retrieval) time while the other time level is the only ‘‘comparison time.’’ Thus,  $M = 1$ , and the weighting function appears as an irrelevant multiplicative factor in  $J$  that can be removed from the problem by division. Experiments with three and more time levels of data (i.e., two or more comparison times,  $M \geq 2$ ) confirm that having the weight decay with time offers a slight benefit over holding the weight constant.

Since  $J_1$  and  $J_2$  have the same dimensions and measure discrepancies in a velocity component (radial velocity in  $J_1$ , azimuthal velocity in  $J_2$ ),  $\mu$  is just the relative weight of the background constraint to the dy-

namical constraint. As described in section 3, in some experiments the background constraint is only imposed in regions where the error in the VVP-like background winds is expected to be low, that is, in regions where the linear wind model is expected to be valid. In regions where these background winds are not trusted ( $Q > 0.5$ ), no background constraint is used ( $\mu = 0$ ). Moreover, even in regions where the background constraint is imposed ( $Q < 0.5$ ),  $\mu$  is set to a very small value ( $\mu = 0.01$ ), which gives relatively little weight to the background winds even in regions where they are trusted. However, tests with this and other datasets have shown that in regions where the topography of the first cost function alone tends to be relatively flat, the addition of even a relatively small background term has a large impact.

Throughout our preliminary testing, we minimized  $J$  by brute force, that is, by explicitly evaluating  $J$  for a wide range of the three control variables. Although such a procedure would be too slow for operational purposes, it was valuable for research purposes since it allowed us to visualize the  $J$  topography (through contour plots) and thereby explore the threat of solution nonuniqueness. More recently we have adopted a standard steepest descent algorithm that rapidly locates a local minimum for  $J$ . To start this iterative procedure, a first guess must be imposed for each of the control variables. A first guess of zero is used for the radial forcing and polar velocity component. The first guess for the azimuthal velocity component is the azimuthal component of a single-Doppler retrieved ‘‘sounding’’ velocity obtained from a VVP-like calculation in which the sounding wind is restricted to be constant within layers 100 m thick extending across the whole analysis domain (i.e., the data are binned into 100-m-wide layers). Of course, if the retrieval yields a unique result, then the retrieved variables must be independent of these first guesses.

## 5. Retrieval test case: 16 June 2000 cold front

### a. Overview of the 16 June 2000 dataset

The single-Doppler velocity retrieval technique was tested with data gathered by two of the DOW radars observing a slow-moving cold front late on the afternoon of 16 June 2000 near Grandfield, Oklahoma. At the surface, the cold front extended from a low pressure system over west-central Quebec, Canada, southwestward through the central United States to New Mexico. Across southwestern Oklahoma, near Grandfield, the front was moving southward at approximately 2–3 m s<sup>-1</sup>. Surface winds were from the southeast at ~5–10 m s<sup>-1</sup> south of the front and from the northeast at ~5–10 m s<sup>-1</sup> north of the front. Skies were cloudy but no precipitation was observed during the radar deployment.

Radial velocity data from one DOW (hereafter referred to as the ‘‘input’’ radar) were supplied to the retrieval while radial velocity data from both DOWs

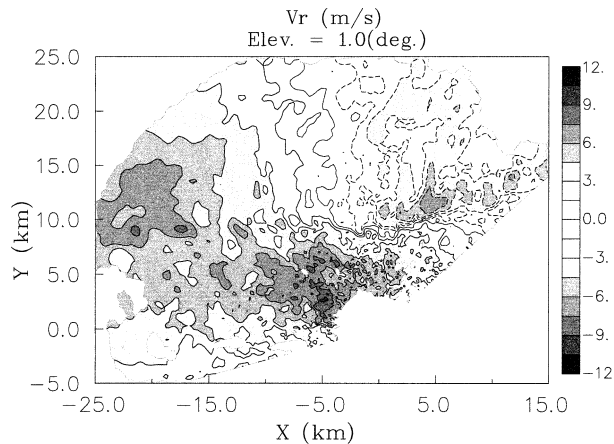


FIG. 2. Analyzed radial velocity field from the input radar on the  $\theta = 1^\circ$  surface at 2254:49 UTC 16 Jun 2000. Input radar is at  $x = 0$ ,  $y = 0$ . Contour increment =  $1.5 \text{ m s}^{-1}$ . Negative contours dashed.

were used to generate the dual-Doppler wind analysis used to verify the results. The low-level ( $\theta = 1^\circ$ ) radial velocity field from the input radar at the retrieval time 2254:49 UTC is presented in Fig. 2. The input radar coincides with the origin ( $x = 0$ ,  $y = 0$ ), and the second radar is at  $x = -17.64 \text{ km}$ ,  $y = 0.96 \text{ km}$ . The dual-Doppler analyzed vector wind field interpolated to the  $z = 300 \text{ m}$  surface of a Cartesian grid at this same time is presented in Fig. 3. The dual-Doppler analysis shows a convergent frontal zone extending across the southern part of the domain, with peak wind speeds approaching  $12 \text{ m s}^{-1}$  in the northeasterly flow behind the front. The azimuthal component of the dual-Doppler wind field is displayed on the  $\theta = 1^\circ$  surface of the input radar grid in Fig. 4.

#### b. Data processing

Data from each radar were gathered in sector volumes of  $150^\circ$  azimuthal width extending radially outward  $\sim 28 \text{ km}$  and ranging in elevation angle from  $\theta = 0.2^\circ$  to  $9.0^\circ$ . Complete sector-volume scans were obtained at time intervals ranging between 57 and 59 s (for simplicity we will refer to these as 1-min intervals, although we did use the exact values in the retrieval experiments), with a range spacing of  $\Delta r = 99 \text{ m}$ , an azimuthal angle spacing of  $\Delta \phi = 0.25^\circ$ , and a variable elevation angle spacing ranging from  $\Delta \theta \sim 0.7^\circ$  near the lower surface up to  $\sim 1.6^\circ$  at the top of the sector volume. Data on the lowest elevation angle suffered from significant ground clutter contamination, and were used only for orientation purposes (ground clutter provided a useful map of reference targets to help orient the grid of data points from the two radars). The lowest elevation angle on which data were actually used in the retrieval was the second level,  $\theta = 1^\circ$ .

The raw radial velocity data were manually edited using Solo software (Oye et al. 1995) to remove residual

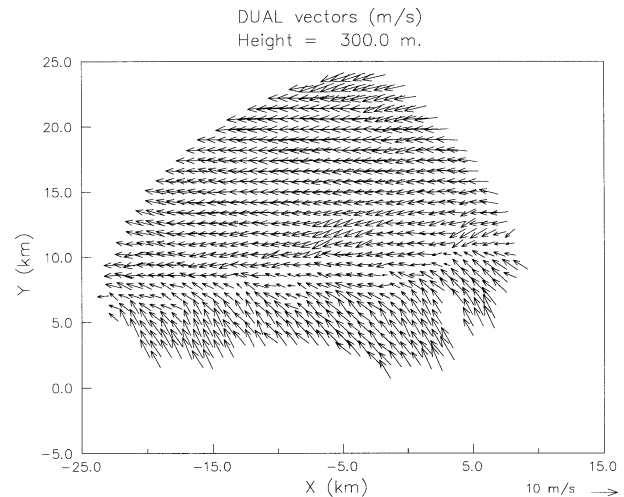


FIG. 3. Dual-Doppler analyzed wind vectors interpolated to the  $z = 300 \text{ m}$  surface at 2254:49 UTC 16 Jun 2000. Peak wind speeds  $\sim 12 \text{ m s}^{-1}$ .

ground clutter contamination and isolated pixels of radial velocity data that differed significantly from nearest-neighbor values. A three-dimensional Barnes analysis was then used to interpolate the edited winds from both radars to the retrieval grid—a coarser regularly spaced spherical polar grid centered on the input radar with radial, azimuthal, and elevation angle grid spacings of  $\Delta r = 250 \text{ m}$ ,  $\Delta \phi = 1.0^\circ$ , and  $\Delta \theta = 0.7^\circ$ , respectively. The Barnes parameters defined a data ellipsoid that was isotropic (circular) in the conical ( $r$ ,  $\phi$ ) surface. The quasi-horizontal radius of influence extended across  $0.7^\circ$  in azimuth, and the quasi-horizontal cutoff radius extended across  $2.0^\circ$  in azimuth. The corresponding polar ( $\theta$ ) radius of influence and polar cutoff radius extended across  $0.3^\circ$  and  $0.6^\circ$  of the elevation angle, respectively. These angular values were multiplied by the radius  $r$  to get physical lengths for the influence/cutoff radii.

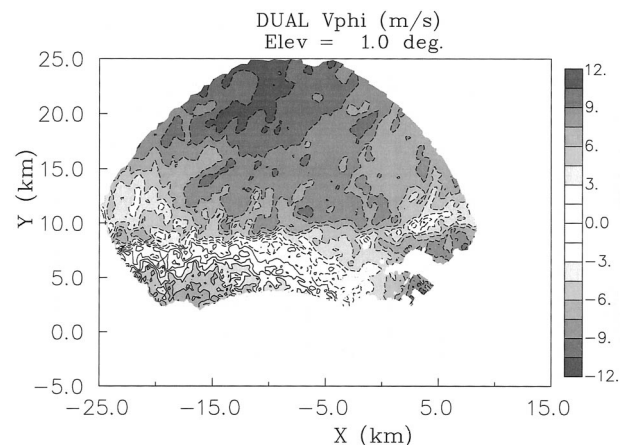


FIG. 4. Azimuthal component of the dual-Doppler analyzed wind field on the  $\theta = 1^\circ$  surface. Contour increment =  $1.5 \text{ m s}^{-1}$ . Negative contours dashed.

Since the radii of influence and cutoff radii were based on a fixed angle spacing, their physical lengths decreased with decreasing radius, and fewer range gates of data were incorporated into the analysis at smaller radii. The specification of these radii were amended so that there would always be at least three range gates of data entering the analysis at any analysis point. This was accomplished in an ad hoc manner by “freezing” the physical lengths of all radii of influence and cutoff radii for all  $r$  less than the radius  $r^*$  at which only three range gates of data would enter the analysis calculation. The radius  $r^*$  was approximately 6 km for this dataset.

Because of the likelihood for bias in the analyzed radial velocity data near regions of missing data (particularly near upper or lower data boundaries in conditions of strong wind shear), analyzed values were rejected if the surrounding data distribution was highly asymmetric. Each data ellipsoid was partitioned into four quasi-horizontal quadrants, and the corresponding analyzed value was rejected if there was less than 5% raw data coverage within any quadrant or if there was less than 20% raw data coverage within either the upper or lower halves of the ellipsoid (unless there were raw data points within  $0.2^\circ$  of elevation angle of the analysis point).

For each experiment analyzed radial velocity data from the input radar were supplied to the retrieval, and the retrieved azimuthal wind component  $u_{\phi 0}$  was compared with the azimuthal wind component obtained from a dual-Doppler wind analysis (dual-Doppler wind vectors projected into the azimuthal direction). The dual-Doppler analysis was performed on the retrieval grid with radial velocity data interpolated from both radars following the analysis procedure described above. A statistical verification of the retrieved azimuthal velocity component was then performed on the retrieval grid, as described in section 5b. A qualitative verification was also performed by making pictures of the retrieved and dual-Doppler analyzed azimuthal velocity component on the retrieval grid. Wind vector plots were also examined. However, the inhomogeneous spacing of the wind vectors on the spherical polar grid (especially the crowding of vectors near the radar) made the spherical display less suitable for illustrating the qualitative features of the flow than did a Cartesian display. Accordingly, for visualization purposes only, the retrieved and dual-Doppler analyzed wind vectors were interpolated to a regular Cartesian grid (as in Fig. 3).

### c. Retrieval experiments

The experiments described herein were designed to study the impact of rapid-scan radar data on retrieval accuracy, and to assess the sensitivity of the retrieval to selective application of the background wind constraint. All experiments had a common retrieval time ( $t = 0$ ) corresponding to 2254:49 UTC 16 June 2000. The default retrieval patch width subtended  $8^\circ$  of azimuth,

which corresponded to sides of length 700 m at a close range of 5 km, and sides of length 3.5 km at a far range of  $r = 25$  km. The patch width for the background wind calculation subtended  $30^\circ$  of azimuth.

For each experiment the root-mean-square error (rmse) in the retrieved azimuthal wind  $u_{\phi 0}$  and the correlation coefficient COR of the retrieved azimuthal wind  $u_{\phi 0}$  and the azimuthal component of the dual-Doppler wind  $u_{\phi \text{dual}}$  were computed on the retrieval grid as a function of elevation angle. On each elevation angle we defined the average of a variable  $F$  by  $\bar{F} \equiv \sum_{n=1}^N \Delta v F_n / \sum_{n=1}^N \Delta v$ , where  $N$  was the number of grid points for which both retrieved and dual-Doppler analyzed winds were available,  $F_n$  was the value of  $F$  at the  $n$ th grid point, and  $\Delta v \equiv r^2 \cos \theta \Delta r \Delta \theta \Delta \phi$  was a differential volume element. With this notation, rmse and COR were defined as follows:

$$\text{rmse} \equiv \overline{(u_{\phi 0} - u_{\phi \text{dual}})^2}^{1/2} \quad \text{and} \quad (27)$$

$$\text{COR} \equiv \frac{\overline{(u_{\phi 0} - \bar{u}_{\phi 0})(u_{\phi \text{dual}} - \bar{u}_{\phi \text{dual}})}}{\overline{(u_{\phi 0} - \bar{u}_{\phi 0})^2}^{1/2} \overline{(u_{\phi \text{dual}} - \bar{u}_{\phi \text{dual}})^2}^{1/2}}. \quad (28)$$

Test results will be presented for the lowest elevation angle ( $\theta = 1^\circ$ ) and as an average over all data points ( $\theta = 1^\circ - 8.7^\circ$ ).

The first five experiments used two time levels of data of progressively degraded (coarsened) temporal resolution. The background constraint was turned off everywhere. The first time level was at  $t = 0$ , while the second time level corresponded to  $t = \Delta t$ , where  $\Delta t = 1, 2, 3, 4,$  and  $5$  min, respectively. The 5-min time resolution of this last experiment matched the shortest operational scanning period of the WSR-88Ds (Klazura and Imy 1993). The results presented in Fig. 5 show that time resolution has a significant impact on retrieval skill. At the lowest level, the rmse decreased by  $\sim 35\%$  from  $4.74 \text{ m s}^{-1}$  at the 5-min resolution to  $3.08 \text{ m s}^{-1}$  at the 1-min resolution, while COR increased by  $\sim 60\%$  from 0.53 at the 5-min resolution to 0.86 at the 1-min resolution. Contour plots of  $J$  obtained by explicitly evaluating  $J$  for a wide range of values of  $u_{\phi 0}$  and  $a_{r0}$  were helpful in diagnosing these results. Inspection of contour plots at many analysis points revealed that the  $J$  topography associated with data of low temporal resolution ( $\Delta t = 5$  min) was typically fraught with multiple minima, whereas the  $J$  topography associated with data of high temporal resolution ( $\Delta t = 1$  min) typically had just one minimum. The situation is well illustrated in Fig. 6, which depicts the sequence of contour plots of  $J$  for a selected analysis point in the frontal convergence zone ( $x = 1$  km,  $y = 10$  km) on the lowest elevation angle ( $\theta = 1^\circ$ ) at various temporal resolutions.<sup>1</sup> Distinct

<sup>1</sup> The  $J$  topography in Fig. 6 was calculated with  $u_{\theta 0}$  explicitly set to zero (which we deemed reasonable since the analysis point was near the ground). The dual-Doppler analyzed value of  $w$  at this point was on the order of  $0.25 \text{ m s}^{-1}$ .

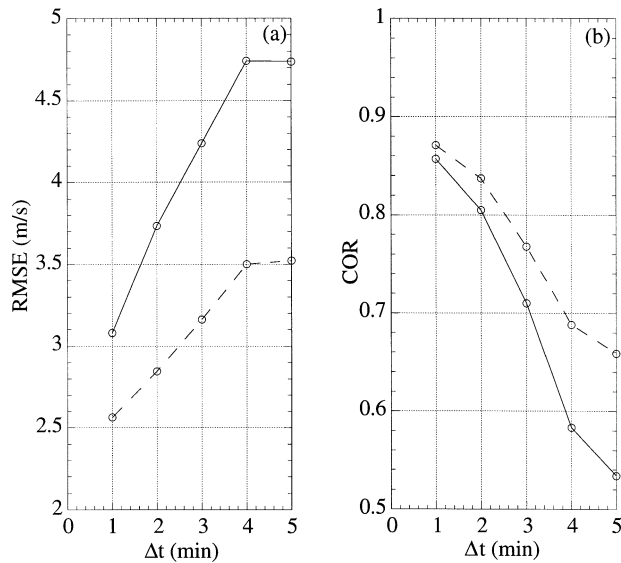


FIG. 5. Retrieved azimuthal wind statistics as functions of  $\Delta t$  for the two-time-level experiments with no background constraint: (a) rmse in retrieved azimuthal wind and (b) correlation coefficient (COR) of retrieved and dual-Doppler analyzed azimuthal winds. Results at lowest elevation angle ( $\theta = 1^\circ$ ) are indicated by solid lines; dashed lines are averages over all data points ( $\theta = 1^\circ - 8.7^\circ$ ).

multiple minima appear in the cost function topography at the lower temporal resolutions. Keeping in mind that the dual-Doppler analyzed value of the azimuthal wind at this point was  $-6 \text{ m s}^{-1}$ , we see that the (unique) solution  $u_{\phi 0} = -5.5 \text{ m s}^{-1}$  in the highest temporal resolution experiment was in good agreement with the dual-Doppler analyzed value, while the global minimum solution  $u_{\phi 0} = +14.5 \text{ m s}^{-1}$  in the experiment of lowest temporal resolution was in very serious error. Inspection of these and other cost function plots suggested that the poor rmse and COR values in the low-resolution experiments would actually have been worse had we sought a global minimum (e.g., by brute force evaluation of  $J$ ) instead of a local minimum. This suggests that in the presence of multiple minima, use of a local minimization algorithm initialized with a good first guess may give an unrepresentative and overly optimistic picture of the value added by the dynamical constraint.

The next set of experiments focused on the impact of the background wind constraint. However, before considering the results from these experiments, it is instructive to examine the background winds themselves. The azimuthal component of the background winds on the  $\theta = 1^\circ$  surface of the retrieval grid is presented in Fig. 7. The mean-squared error  $Q$  in the radial component of the background winds on the  $\theta = 1^\circ$  surface is depicted in Fig. 8. In regions where  $Q$  was small (less than our threshold value of 0.5), the azimuthal component of the background wind was typically within  $2 \text{ m s}^{-1}$  of the azimuthal component of the dual-Doppler wind field (Fig. 4), while in regions where  $Q$  was large, the azimuthal component of the background wind could

be in error by as much as  $15 \text{ m s}^{-1}$ . The rmse associated with the azimuthal component of the background winds (imposed everywhere, regardless of the value of  $Q$ ) was  $3.36 \text{ m s}^{-1}$  on the lowest level ( $\theta = 1^\circ$ ) and  $3.85 \text{ m s}^{-1}$  averaged over all data points ( $\theta = 1^\circ - 8.7^\circ$ ), while the COR was 0.76 at the lowest level and 0.75 averaged over all data points.

Presented in Fig. 9 are the results from rerunning the previous two-time-level experiments but with the background wind constraint selectively imposed ( $\mu = 0.01$  in regions where  $Q < 0.5$ , and  $\mu = 0$  in regions where  $Q > 0.5$ ). Clearly, selective application of the background constraint is greatly preferable to nonapplication of the background constraint for all time resolutions. With selective application of the background constraint, the rmse in the experiment with the highest temporal resolution ( $\Delta t = 1 \text{ min}$ ) has dropped to just under  $2.1 \text{ m s}^{-1}$  (at the lowest level and averaged over all levels), while the COR has increased to just over 0.9. Presented in Fig. 10 are the results from rerunning the two-time-level experiments but with the background constraint imposed everywhere (with  $\mu = 0.01$ ). Compared to nonapplication of the background constraint, widespread application of the background constraint also improves the rmse and COR results for all time resolutions (with the exception of the domain average rmse in the  $\Delta t = 1 \text{ min}$  experiment). However, comparing the selective background experiments (Fig. 9) with the full background experiments (Fig. 10) reveals a surprising result: the benefit in selectively applying the background constraint over applying the background constraint everywhere is only realized at the higher temporal resolutions ( $\Delta t = 1 \text{ min}$  and  $\Delta t = 2 \text{ min}$ ). At the relatively low temporal resolutions ( $\Delta t = 4 \text{ min}$  and  $\Delta t = 5 \text{ min}$ ), full application of the background winds is preferable to selective application. The implication of this result is that the dynamical constraint by itself yields such poor results at low temporal resolutions that even the addition of untrustworthy background wind information adds value.

In the next set of experiments the retrieval time window was lengthened by using multiple time levels of data supplied at the highest time resolution ( $\Delta t = 1 \text{ min}$ ). The background constraint was turned off. Experiments were run with two volume scans (the previous run, which used data at  $t = 0$  and  $1 \text{ min}$ ), three volume scans ( $t = 0, 1$ , and  $2 \text{ min}$ ), four volume scans ( $t = 0, 1, 2$ , and  $3 \text{ min}$ ), five volume scans ( $t = 0, 1, 2, 3$ , and  $4 \text{ min}$ ), and six volume scans ( $t = 0, 1, 2, 3, 4$ , and  $5 \text{ min}$ ). As seen in Fig. 11, both the low-level and overall skill in these experiments degraded as more volume scans were used. At the lowest level the rmse steadily increased from  $3.08 \text{ m s}^{-1}$  (with two volume scans) to  $3.83 \text{ m s}^{-1}$  (with six volume scans), while the COR decreased from 0.86 to 0.75. Apparently the extra information provided by multiple volume scans did not offset the deleterious effect of a lengthened time window.

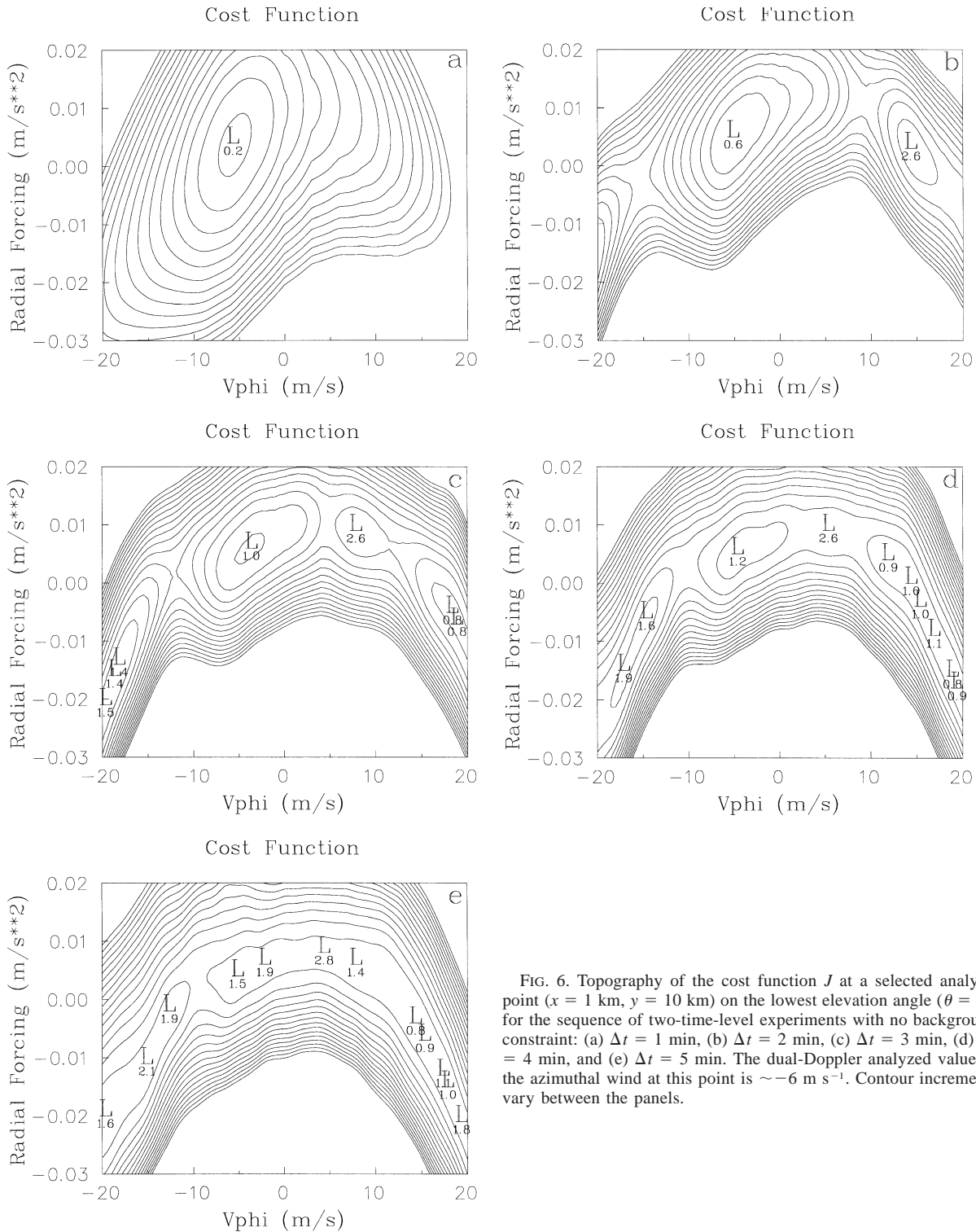


FIG. 6. Topography of the cost function  $J$  at a selected analysis point ( $x = 1$  km,  $y = 10$  km) on the lowest elevation angle ( $\theta = 1^\circ$ ) for the sequence of two-time-level experiments with no background constraint: (a)  $\Delta t = 1$  min, (b)  $\Delta t = 2$  min, (c)  $\Delta t = 3$  min, (d)  $\Delta t = 4$  min, and (e)  $\Delta t = 5$  min. The dual-Doppler analyzed value of the azimuthal wind at this point is  $\sim -6$  m s $^{-1}$ . Contour increments vary between the panels.

The next set of experiments tested the sensitivity of the retrieval to retrieval patch size. The two-time-level experiment with the highest time resolution ( $\Delta t = 1$  min) and no background constraint was rerun with the patch width changed from the original  $8^\circ$  to a range of

values between  $0^\circ$  (i.e., a single point, no patch) and  $24^\circ$ . As seen in Fig. 12, use of a patch clearly improved both rmse (which dropped from an overall value of  $3.40$  m s $^{-1}$  with no patch to  $2.36$  m s $^{-1}$  with a  $16^\circ$  patch) and COR (which increased from an overall value of  $0.75$

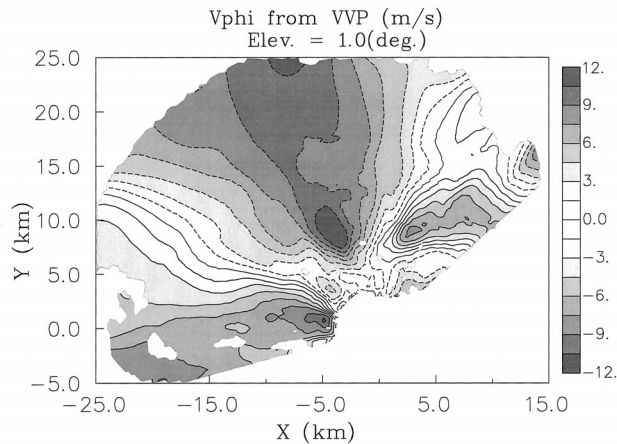


FIG. 7. Azimuthal component of the background wind field on the  $\theta = 1^\circ$  surface. Contour increment =  $1.5 \text{ m s}^{-1}$ . Negative contours dashed.

with no patch to 0.91 with a  $24^\circ$  patch). The patch was used to stabilize estimates of the wind field in the presence of noisy data, though this came at the expense of spatial resolution. Other methods of controlling noise are common in the literature: Xu et al. (2001) used spline representations to filter short-wave noise; Xu et al. (1994b), Shapiro et al. (1995), and Weygandt et al. (2002a) used large values of Cressman radius to smooth the input data in an analysis step prior to the retrieval; Sun and Crook (1994), Laroche and Zawadzki (1995), and Gao et al. (2001) included explicit smoothness constraints (penalty terms) within their retrieval algorithms.

The best results obtained thus far were found in the two-time-level experiment of highest time resolution ( $\Delta t = 1 \text{ min}$ ) with selective application of the background constraint. This experiment had the smallest magnitude of  $t$ . However, by using both forward and

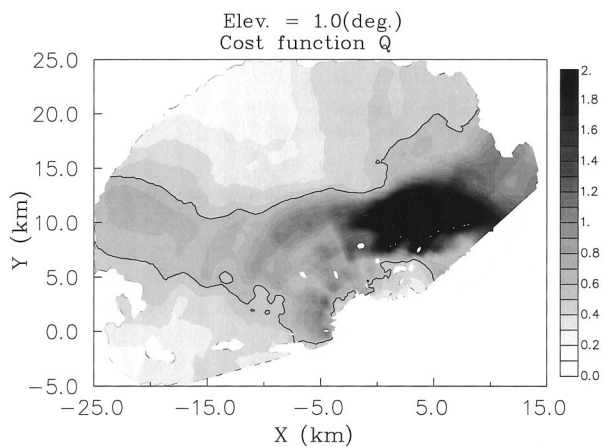


FIG. 8. Mean-squared error  $Q$  in the radial component of the background wind field on the  $\theta = 1^\circ$  surface. The 0.5 contour (solid line) is the threshold for selective application of the background constraint. Contour increment =  $0.1 \text{ m}^2 \text{ s}^{-2}$ .

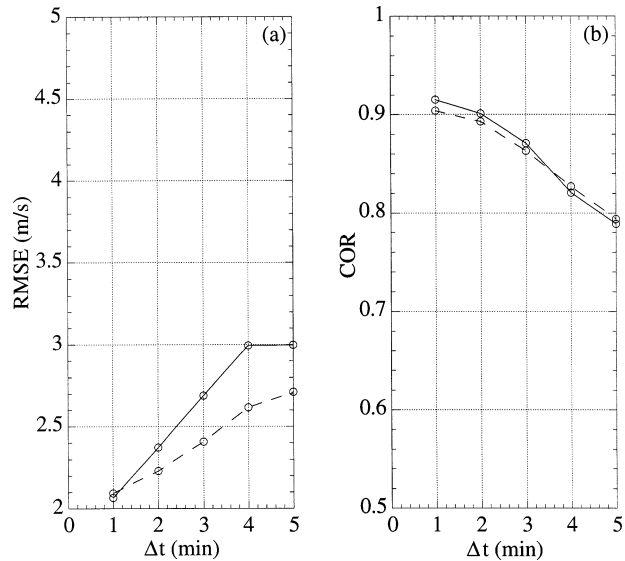


FIG. 9. As in Fig. 5 but for the experiments where the background constraint is selectively imposed.

backward trajectories, additional information could be brought into the retrieval while leaving the maximum magnitude of  $t$  unchanged. To see whether use of both forward and backward trajectories would improve on our previous best results, we ran a three-time-level experiment using data of the highest time resolution ( $\Delta t = 1 \text{ min}$ ) and a selectively imposed background constraint. Trajectories originated from the  $t = 0$  retrieval time and ran forward and backward in time by 1 min. Surprisingly, the overall rmse in this experiment,  $2.04 \text{ m s}^{-1}$ , was only slightly lower than the  $2.10 \text{ m s}^{-1}$  rmse in the corresponding forward-only experiment, while

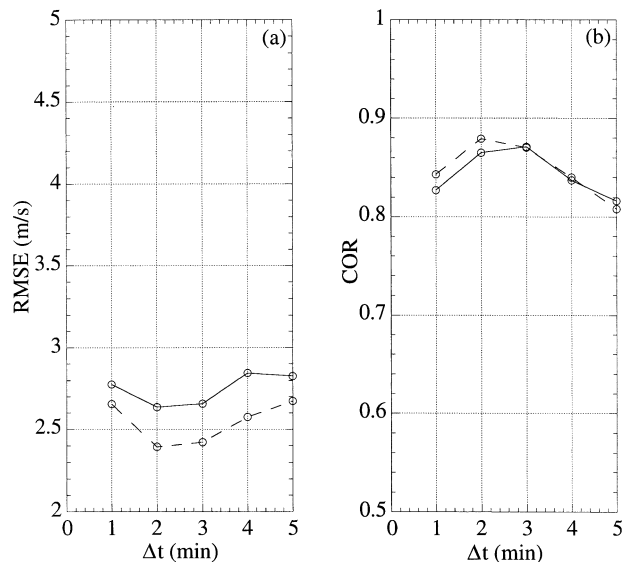


FIG. 10. As in Fig. 5 but for the experiments where the background constraint is imposed everywhere.

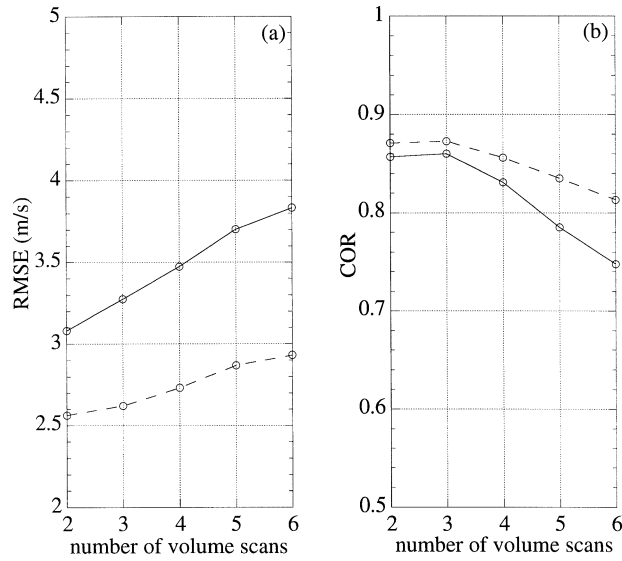


FIG. 11. Retrieved azimuthal wind statistics as functions of the number of input volume scans. These experiments were performed with  $\Delta t = 1$  min, and no background constraint: (a) rmse in retrieved azimuthal wind and (b) COR of retrieved and dual-Doppler analyzed azimuthal winds. Results at lowest elevation angle ( $\theta = 1^\circ$ ) are indicated by solid lines; dashed lines are averages over all data points ( $\theta = 1^\circ - 8.7^\circ$ ).

the low-level rmse of  $2.06 \text{ m s}^{-1}$  had hardly changed from the value of  $2.07 \text{ m s}^{-1}$  in the forward-only experiment. The low-level COR was unchanged at 0.92, while the overall average COR had improved slightly to 0.92 from 0.90.

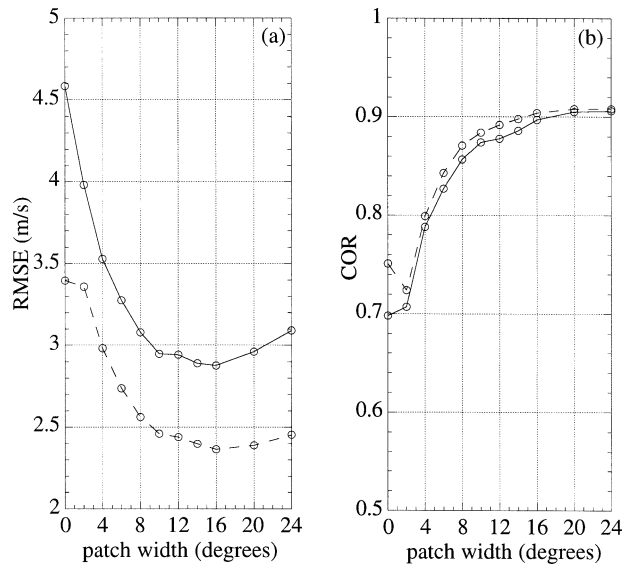


FIG. 12. Retrieved azimuthal wind statistics as functions of azimuthal patch width for the two-time-level experiments of highest temporal resolution ( $\Delta t = 1$  min) with no background constraint: (a) rmse in retrieved azimuthal wind and (b) COR of retrieved and dual-Doppler analyzed azimuthal winds. Results at lowest elevation angle ( $\theta = 1^\circ$ ) are indicated by solid lines; dashed lines are averages over all data points ( $\theta = 1^\circ - 8.7^\circ$ ).

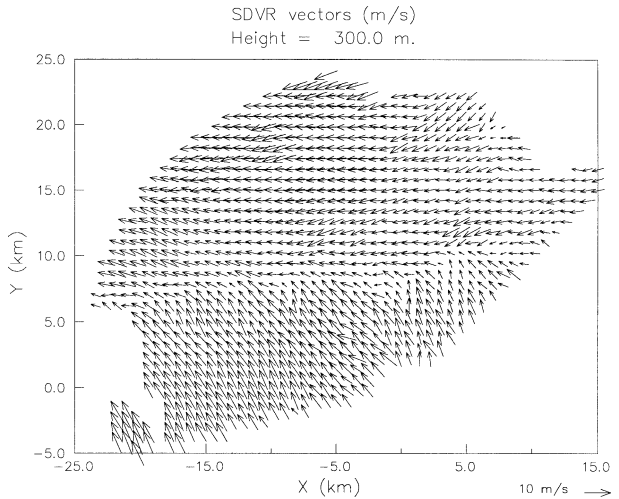


FIG. 13. Single-Doppler retrieved wind vectors interpolated to the  $z = 300$  m surface. Results are from the two-time-level experiment of highest temporal resolution ( $\Delta t = 1$  min) with the background constraint selectively imposed. Peak wind speeds  $\sim 10 \text{ m s}^{-1}$ .

Wind vectors from the two-time-level experiment of highest time resolution ( $\Delta t = 1$  min) with selective application of the background constraint are presented in Fig. 13. The retrieved velocity field is in good qualitative agreement with the dual-Doppler analyzed velocity field (Fig. 3). Moreover, the retrieved azimuthal wind component (Fig. 14) compares favorably with the azimuthal component of the dual-Doppler analyzed winds (Fig. 4). The retrieval has successfully recovered the gross features of the flow, namely, the convergent zone in the southern part of the domain, the strong northeasterly winds in the northern part of the domain, and the southeasterly winds in the southern part of the domain. A more stringent verification

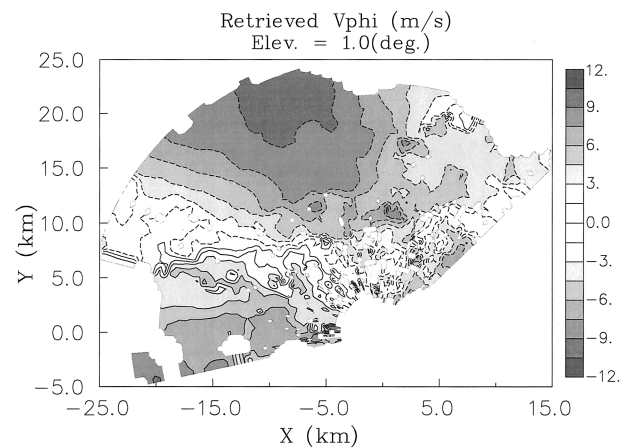


FIG. 14. Retrieved azimuthal wind component on the  $\theta = 1^\circ$  surface. Results are from the two-time-level experiment of highest temporal resolution ( $\Delta t = 1$  min) with the background constraint selectively imposed. Contour increment =  $1.5 \text{ m s}^{-1}$ . Negative contours dashed.

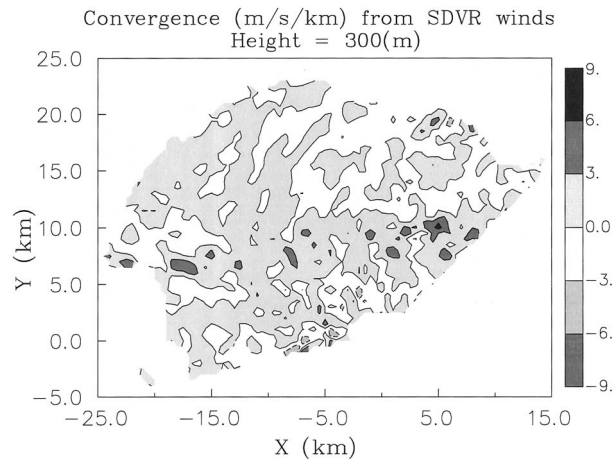


FIG. 15. Horizontal convergence of single-Doppler retrieved wind field on the  $z = 300$  m surface. Results are from the two-time-level experiment of highest temporal resolution ( $\Delta t = 1$  min) with background constraint selectively imposed. Negative contours dashed.

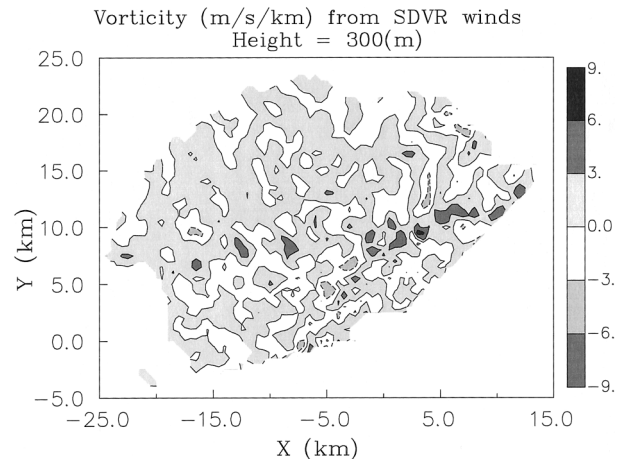


FIG. 17. Vertical vorticity obtained from single-Doppler retrieved winds on the  $z = 300$  m surface. Results are from the two-time-level experiment of highest temporal resolution ( $\Delta t = 1$  min) with background constraint selectively imposed. Negative contours dashed.

can be made by comparing the horizontal convergence of the retrieved wind  $-(\partial u/\partial x + \partial v/\partial y)$  (Fig. 15) with the horizontal convergence obtained from the dual-Doppler analysis (Fig. 16). Results are presented on the  $z = 300$  m surface. The single-Doppler retrieved horizontal convergence was obtained by interpolating the retrieved spherical wind components on the spherical grid to the Cartesian grid, converting to Cartesian wind components, and then differentiating the Cartesian wind components on the Cartesian grid. Although there are discrepancies in the details between the retrieved and dual-Doppler analyzed convergence fields, the retrieval captures the correct magnitude and orientation of the band of high convergence running across the frontal zone (along  $y = 7$  km). The retrieved vertical vorticity  $\partial v/\partial x - \partial u/\partial y$  (Fig. 17) and the vertical vorticity obtained from the dual-Doppler wind analysis (Fig. 18) are also found to be in good

qualitative agreement, at least for the main feature of interest (frontal zone).

A detailed inspection of the rmse and COR statistics for these experiments revealed that the retrieval tended to improve with elevation angle. We suspect that this result is related to the specific variation of flow characteristics with height in this dataset rather than to any intrinsic property of the retrieval algorithm. Since this dataset encompasses the leading edge of the cold front (a shallow system), there is more “structure” in the radial velocity fields at low-elevation angles than at upper-elevation angles (where the radar beams are primarily above the front, in a region of relatively uniform flow). Since the timescales  $T$  and  $L/U$  should be smaller at these lower levels, the rapid-scan condition [upper bound in (17)] should be more restrictive there, that is, the rapid-scan condition would be more likely to be violated at lower levels than at upper levels. However,

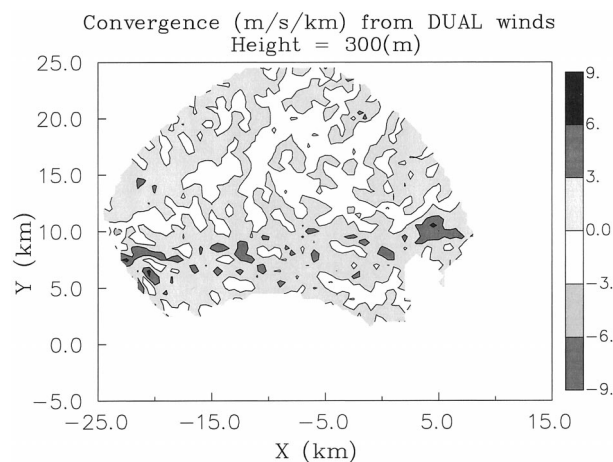


FIG. 16. Dual-Doppler analyzed horizontal convergence on the  $z = 300$  m surface. Negative contours dashed.

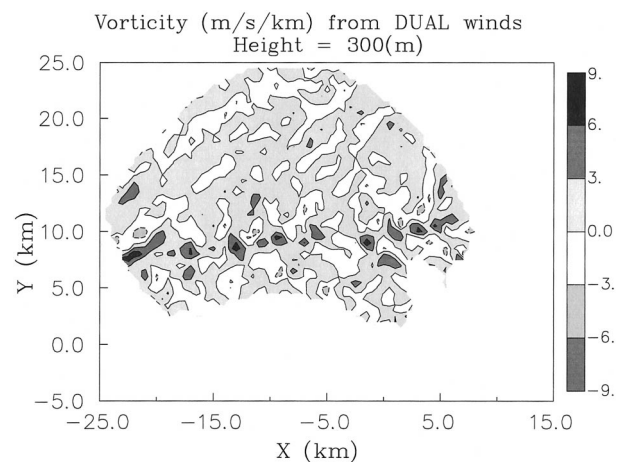


FIG. 18. Dual-Doppler analyzed vertical vorticity on the  $z = 300$  m surface. Negative contours dashed.

this explanation is incomplete because the smaller values of these timescales at lower levels would also make the lower bound in (17) less restrictive. A more rigorous analysis using a procedure to accurately estimate  $L$ ,  $U$ ,  $T$ , and  $\varepsilon$  would help clarify this situation.

Finally, a word is in order concerning the retrieved polar velocity component  $u_{\theta 0}$ . When  $u_{\theta 0}$  is retrieved through the minimization of (24), neither the mass conservation equation nor the lower boundary condition (impermeability condition) are imposed. We have found that the  $u_{\theta 0}$  thus obtained is generally inferior to the  $u_{\theta 0}$  obtained by integrating the mass conservation equation upward from the ground using the convergence obtained from the single-Doppler retrieved winds (more precisely, with  $w$  obtained from the retrieved horizontal convergence, and  $u_{\theta 0}$  then recovered from the full wind vector). In the present case, integrating the retrieved convergence upward from the ground to the  $z = 300$  m surface yields a vertical motion pattern that is very similar to the retrieved convergence pattern in Fig. 15. Similarly, the vertical velocity field on the  $z = 300$  m surface obtained by integrating the dual-Doppler analyzed convergence is very similar to the convergence pattern in Fig. 16. The magnitudes of these retrieved and dual-Doppler analyzed vertical velocity fields are comparable: both attain peak positive values of  $\sim 3$  m s<sup>-1</sup> along the front. Our omission of a mass conservation constraint in (24) was desirable for research purposes since it facilitated our analysis of the cost function topography. However, in real applications, it would likely be preferable to include the mass conservation equation as an additional (simultaneous) constraint, as in Gao et al. (2001) and Xu et al. (2001), or in a postprocessing step to obtain the vertical velocity from the horizontal convergence.

## 6. Summary comments

This study is concerned with application of a single-Doppler velocity retrieval technique to “rapid scan” Doppler radar data. The retrieval combines elements of the Xu et al. (1994b, 1995) and Gao et al. (2001) simple adjoint retrievals with the Laroche and Zawadzki (1994, 1995) Lagrangian variational retrievals. The dynamical model in our Lagrangian retrieval is an approximate version of the radial component of the equation of motion valid for small time intervals. Since the model is applied to air parcels initially collocated with analysis grid points, parcel trajectories need to be computed as part of the solution. The initial cross-beam wind components and initial radial component of the forcing in the equation of motion are treated as unknown parameters (control variables) that need to be retrieved. To reduce retrieval noise, the control variables are frozen over small sectors or “patches” of analysis points. Provision is also made for a selectively imposed background wind constraint obtained from a piecewise linear wind model (a variant of VVP).

The validity of the rapid-scan model is quantified by the inequalities in (17), which restrict the duration of appropriate retrieval time windows. The time window should be smaller than the effective timescale, which is the smallest of (i) the intrinsic (evolution) timescale, (ii) the advection timescale based on characteristic speed and length scales, and (iii) the advection timescale based on the characteristic speed scale and distance from the radar. On the other hand, the time window should be larger than the product of the effective timescale and the relative error  $\varepsilon$  in the radial velocity data (ratio of radial velocity error to characteristic velocity scale). One of the implications of (17) is that for a large enough data error, the rapid-scan model may not be suitable for any time window.

Experiments were performed and verified with data of a cold front observed by the Doppler-on-Wheels radars on 16 June 2000 with a scanning rate of approximately one sector volume per minute. The sensitivity of the retrieval to time resolution was assessed by using data of the highest available temporal resolution ( $\Delta t = 1$  min) and data of progressively degraded temporal resolution. Other experiments examined the sensitivity of the retrieval to length of retrieval time window, application of a background constraint, and retrieval patch size. Key findings with this dataset include the following.

- 1) Retrieval skill could be markedly improved by using data of the highest temporal resolution ( $\Delta t = 1$  min). The cost function associated with the dynamical constraint alone was prone to multiple minima (solution non-uniqueness) when using data of low temporal resolution ( $\Delta t \geq 3$  min).
- 2) When using forward trajectories, the best results were obtained with the smallest retrieval time windows. Use of both forward and backward trajectories improved retrieval skill very slightly.
- 3) Use of a patch of points over which the control variables are frozen reduced noise and improved retrieval skill. Significant error reduction could be obtained with a patch width as small as a few degrees in azimuth. It was hypothesized that use of the patch may improve retrieval accuracy by reducing the effective value of relative error  $\varepsilon$  in (17).
- 4) Use of a background field from a VVP-like estimate of the wind field improved retrieval skill regardless of whether the background constraint was selectively imposed or imposed everywhere. However, the selective approach was superior when the retrieval was performed with data of high temporal resolution.

The inequalities in (17) and our experimental results suggest that algorithms based on the radial component of the equation of motion with stationary or “frozen” bulk forcings may find their greatest utility when used with accurate data of high temporal resolution. However, even in situations where the rapid scan inequality is violated, (17) might be used to guide the filtering of

spatial scales (increasing the effective  $L$ ). In cases where the effective time resolution is dictated by advection rather than by evolution, the spatial resolution might be appropriately degraded so as to allow (17) to be satisfied. However, it is important to note that the length, time, and velocity scales appearing in (17) may vary substantially throughout the flow domain (as well as varying with time), and their characterization may not be straightforward. We speculate that a spectral analysis of the radial velocity field (in space and possibly time) may be useful here. Future work will focus on determining objective local measures of the characteristic time and length scales appearing in (17) and on using this information to filter the input data and to identify regions where the retrieved winds can and cannot be trusted.

*Acknowledgments.* This research was supported by the Coastal Meteorology Research Program (CMRP) under Grant N00014-96-1-1112 from the Office of Naval Research (ONR), by the Center for Analysis and Prediction of Storms (CAPS) under Grant ATM91-20009 from the National Science Foundation (NSF), and by NSF ATM-0129892. One of us (J.G.) was also supported by NSF ATM-9909007. The Doppler-on-Wheels program is a collaboration between the University of Oklahoma (OU) and the National Center for Atmospheric Research (NCAR), supported by NSF and ONR. Discussions with Bill Martin, Curtis Alexander, Seon-Yong Lee, and David Mechem are gratefully acknowledged. Curtis Alexander, MyShelle Bryant, Bill Martin, Steve McDonald, Yvette Richardson, and Paul Ritter assisted with the 16 June 2000 Doppler-on-Wheels field deployment. The Solo software package used for the display and editing of the radar data was developed by the Research Data Program (RDP) of the Atmospheric Technology Division (ATD) at NCAR. Contour plots were prepared with ZXPLLOT graphics software developed by Ming Xue. Tim Kwiatkowski and Mark Lauferweiller provided computer assistance.

## APPENDIX

### Radial Component of the Equation of Motion

In spherical polar coordinates, the radial component of the equation of motion for a fluid can be written as (e.g., Kundu and Cohen 2002)

$$\frac{du_r}{dt} - \frac{u_\phi^2 + u_\theta^2}{r} = a_r, \quad (\text{A1})$$

where  $d/dt \equiv \partial/\partial t + (\mathbf{u} \cdot \nabla)$  is the total derivative operator, and  $a_r$  is the sum of the pressure gradient force and friction terms. Multiplying (A1) by  $r$  and using the fact that  $r(du_r/dt) = d(ru_r)/dt - u_r(dr/dt) = d(ru_r)/dt - u_r^2$ , we obtain,

$$\frac{d(ru_r)}{dt} = u_r^2 + u_\phi^2 + u_\theta^2 + ra_r. \quad (\text{A2})$$

For small values of  $t$ , (A2) can be approximated as

$$\frac{r(t)u_r(t) - r_0u_{r,0}}{t} = u_{r,0}^2 + u_{\phi,0}^2 + u_{\theta,0}^2 + r_0a_{r,0}, \quad (\text{A3})$$

where the total derivative term has been discretized with an uncentered (forward) time difference, and a subscript 0 denotes a value at  $t = 0$ . Multiplying (A3) by  $t$  and rearranging, we obtain

$$u_r(t) = \frac{1}{r(t)}[r_0u_{r,0} + (u_{r,0}^2 + u_{\phi,0}^2 + u_{\theta,0}^2 + a_{r,0}r_0)t], \quad (\text{A4})$$

which is our approximate (rapid scan) radial wind model (21).

## REFERENCES

- Armijo, L., 1969: A theory for the determination of wind and precipitation velocities with Doppler radars. *J. Atmos. Sci.*, **26**, 570–573.
- Atlas, D., Ed., 1990: *Radar in Meteorology*. Amer. Meteor. Soc., 806 pp.
- Boccippio, D. J., 1995: A diagnostic analysis of the VVP single-Doppler retrieval technique. *J. Atmos. Oceanic Technol.*, **12**, 230–248.
- Brandes, E. A., 1977: Flow in severe thunderstorms observed by dual-Doppler radar. *Mon. Wea. Rev.*, **105**, 113–120.
- Browning, K. A., and H. Wexler, 1968: A determination of kinematic properties of a wind field using Doppler-radar. *J. Appl. Meteor.*, **7**, 105–113.
- Caton, P. A. F., 1963: Wind measurement by Doppler radar. *Meteor. Mag.*, **92**, 213–222.
- Caya, A., S. Laroche, I. Zawadzki, and T. Montmerle, 2002: Using single-Doppler data to obtain a mesoscale environmental field. *J. Atmos. Oceanic Technol.*, **19**, 21–36.
- Caya, D., and I. Zawadzki, 1992: VAD analysis of nonlinear wind fields. *J. Atmos. Oceanic Technol.*, **9**, 575–587.
- Friedrich, K., and M. Hagen, 2001: Wind vector field determination with bistatic multiple-Doppler radar network. Preprints, *30th Int. Conf. on Radar Meteorology*, Munich, Germany, Amer. Meteor. Soc., 133–135.
- Gal-Chen, T., 1982: Errors in fixed and moving frame of references: Applications for conventional and Doppler radar analysis. *J. Atmos. Sci.*, **39**, 2279–2300.
- Gao, J., M. Xue, A. Shapiro, and K. K. Droegemeier, 1999: A variational method for the analysis of three-dimensional wind fields from two Doppler radars. *Mon. Wea. Rev.*, **127**, 2128–2142.
- , —, —, Q. Xu, and K. K. Droegemeier, 2001: Three-dimensional simple adjoint velocity retrievals from single-Doppler radar. *J. Atmos. Oceanic Technol.*, **18**, 26–38.
- Kapitza, H., 1991: Numerical experiments with the adjoint of a non-hydrostatic mesoscale model. *Mon. Wea. Rev.*, **119**, 2993–3011.
- Kessinger, C. J., P. S. Ray, and C. E. Hane, 1987: The Oklahoma squall line of 19 May 1977. Part I: A multiple Doppler analysis of convective and stratiform structure. *J. Atmos. Sci.*, **44**, 2840–2864.
- Klazura, G. E., and D. A. Imy, 1993: A description of the initial set of analysis products available from the NEXRAD WSR-88D system. *Bull. Amer. Meteor. Soc.*, **74**, 1293–1311.
- Koscielny, A. J., R. J. Doviak, and R. Rabin, 1982: Statistical considerations in the estimation of divergence from single-Doppler radar and application to prestorm boundary-layer observations. *J. Appl. Meteor.*, **21**, 197–210.

- Kundu, P. K., and I. M. Cohen, 2002: *Fluid Mechanics*. Academic Press, 730 pp.
- Laroche, S., and I. Zawadzki, 1994: A variational analysis method for retrieval of three-dimensional wind field from single-Doppler radar data. *J. Atmos. Sci.*, **51**, 2664–2682.
- , and —, 1995: Retrievals of horizontal winds from single-Doppler clear-air data by methods of cross correlation and variational analysis. *J. Atmos. Oceanic Technol.*, **12**, 721–738.
- Lazarus, S., A. Shapiro, and K. K. Droegemeier, 1999: Analysis of the Gal-Chen–Zhang single-Doppler velocity retrieval. *J. Atmos. Oceanic Technol.*, **16**, 5–18.
- , —, and —, 2001: An application of the Gal-Chen–Zhang single-Doppler velocity retrieval to a deep convective storm. *J. Atmos. Sci.*, **58**, 998–1016.
- Lhermitte, R. M., and D. Atlas, 1961: Precipitation motion by pulse Doppler radar. *Proc. Ninth Weather Radar Conf.*, Kansas City, MO, Amer. Meteor. Soc., 218–223.
- Li, Y., 1991: A note on the uniqueness problem of variational adjustment approach to four-dimensional data assimilation. *J. Meteor. Soc. Japan*, **69**, 581–585.
- Liou, Y.-C., 1999: Single radar recovery of cross-beam wind components using a modified moving frame of reference technique. *J. Atmos. Oceanic Technol.*, **16**, 1003–1016.
- , and I.-S. Luo, 2001: An investigation of the moving-frame single-Doppler wind retrieval technique using Taiwan Area Mesoscale Experiment low-level data. *J. Appl. Meteor.*, **40**, 1900–1917.
- Maddox, R. A., J. Zhang, J. J. Gourley, and K. W. Howard, 2002: Weather radar coverage over the contiguous United States. *Wea. Forecasting*, **17**, 927–934.
- Miller, L. J., and R. G. Strauch, 1974: A dual Doppler radar method for the determination of wind velocities within precipitating weather systems. *Remote Sens. Environ.*, **3**, 219–235.
- Oye, R., C. Mueller, and S. Smith, 1995: Software for radar translation, visualization, editing and interpolation. Preprints, *27th Conf. on Radar Meteorology*, Vail, CO, Amer. Meteor. Soc., 359–361.
- Pereira Fo., A. J., K. C. Crawford, and D. J. Stensrud, 1999: Mesoscale precipitation fields. Part II: Hydrometeorologic modeling. *J. Appl. Meteor.*, **38**, 102–125.
- Probert-Jones, J. R., 1960: Meteorological use of pulse Doppler radar. *Nature*, **186**, 271–273.
- Protat, A., and I. Zawadzki, 1999: A variational method for real-time retrieval of three-dimensional wind field from multiple-Doppler bistatic radar network data. *J. Atmos. Oceanic Technol.*, **16**, 432–449.
- Qiu, C.-J., and Q. Xu, 1992: A simple adjoint method of wind analysis for single-Doppler data. *J. Atmos. Oceanic Technol.*, **9**, 588–598.
- , and —, 1996: Least squares retrieval of microburst winds from single-Doppler radar data. *Mon. Wea. Rev.*, **124**, 1132–1144.
- Ray, P. S., C. L. Ziegler, W. Bumgarner, and R. J. Serafin, 1980: Single- and multiple-Doppler radar observations of tornadic storms. *Mon. Wea. Rev.*, **108**, 1607–1625.
- Rinehart, R. E., 1979: Internal storm motions from a single non-Doppler weather radar. NCAR/TN-146 + STR, 262 pp.
- Sasaki, Y., 1970a: Numerical variational analysis formulated under the constraints as determined by longwave equations and a low-pass filter. *Mon. Wea. Rev.*, **98**, 884–898.
- , 1970b: Numerical variational analysis with weak constraint and application to surface analysis of severe storm gust. *Mon. Wea. Rev.*, **98**, 899–910.
- , 1970c: Some basic formalisms in numerical variational analysis. *Mon. Wea. Rev.*, **98**, 875–883.
- Satoh, S., and J. Wurman, 2003: Accuracy of wind fields observed by a bistatic Doppler radar network. *J. Atmos. Oceanic Technol.*, **20**, 1077–1091.
- Serafin, R. J., and J. W. Wilson, 2000: Operational weather radar in the United States: Progress and opportunity. *Bull. Amer. Meteor. Soc.*, **81**, 501–518.
- Shapiro, A., and J. Mewes, 1999: New formulations of dual-Doppler wind analysis. *J. Atmos. Oceanic Technol.*, **16**, 782–792.
- , S. Ellis, and J. Shaw, 1995: Single-Doppler velocity retrievals with Phoenix II data: Clear air and microburst wind retrievals in the planetary boundary layer. *J. Atmos. Sci.*, **52**, 1265–1287.
- Smythe, G. R., and D. S. Zrnic, 1983: Correlation analysis of Doppler radar data and retrieval of the horizontal wind. *J. Appl. Meteor.*, **22**, 297–311.
- Sun, J., and N. A. Crook, 1994: Wind and thermodynamic retrieval from single-Doppler measurements of a gust front observed during Phoenix II. *Mon. Wea. Rev.*, **122**, 1075–1091.
- , and —, 2001: Real-time low-level wind and temperature analysis using single WSR-88D data. *Wea. Forecasting*, **16**, 117–132.
- , D. W. Flicker, and D. K. Lilly, 1991: Recovery of three-dimensional wind and temperature fields from simulated Doppler radar data. *J. Atmos. Sci.*, **48**, 876–890.
- Tuttle, J. D., and G. B. Foote, 1990: Determination of the boundary layer airflow from a single Doppler radar. *J. Atmos. Oceanic Technol.*, **7**, 218–232.
- Waldeufel, P., and H. Corbin, 1979: On the analysis of single-Doppler radar data. *J. Appl. Meteor.*, **18**, 532–542.
- Weygandt, S. S., A. Shapiro, and K. K. Droegemeier, 2002a: Retrieval of initial forecast fields from single-Doppler observations of a supercell thunderstorm. Part I: Single-Doppler velocity retrieval. *Mon. Wea. Rev.*, **130**, 433–453.
- , —, and —, 2002b: Retrieval of initial forecast fields from single-Doppler observations of a supercell thunderstorm. Part II: Thermodynamic retrieval and model prediction. *Mon. Wea. Rev.*, **130**, 454–476.
- Wilson, J. W., N. A. Crook, C. K. Mueller, J. Sun, and M. Dixon, 1998: Nowcasting thunderstorms: A status report. *Bull. Amer. Meteor. Soc.*, **79**, 2079–2100.
- Wurman, J., 1994: Vector winds from a single transmitter bistatic dual-Doppler radar network. *Bull. Amer. Meteor. Soc.*, **75**, 983–994.
- , 2001: The DOW mobile multiple-Doppler network. Preprints, *30th Int. Conf. on Radar Meteorology*, Munich, Germany, Amer. Meteor. Soc., 95–97.
- , S. Heckman, and D. Boccippio, 1993: A bistatic multiple-Doppler network. *J. Appl. Meteor.*, **32**, 1802–1814.
- , J. M. Straka, E. Rasmussen, M. Randall, and A. Zahrai, 1997: Design and deployment of a portable pencil-beam pulsed Doppler 3-cm radar. *J. Atmos. Oceanic Technol.*, **14**, 1502–1512.
- Xu, Q., C. J. Qiu, and J.-X. Yu, 1994a: Adjoint-method retrievals of low-altitude wind fields from single-Doppler reflectivity measured during Phoenix-II. *J. Atmos. Oceanic Technol.*, **11**, 275–288.
- , —, and —, 1994b: Adjoint-method retrievals of low-altitude wind fields from single-Doppler wind data. *J. Atmos. Oceanic Technol.*, **11**, 579–585.
- , —, H.-D. Gu, and J.-X. Yu, 1995: Simple adjoint retrievals of microburst winds from single-Doppler radar data. *Mon. Wea. Rev.*, **123**, 1822–1833.
- , H. Gu, and C.-J. Qiu, 2001: Simple adjoint retrievals of wet-microburst winds and gust-front winds from single-Doppler radar data. *J. Appl. Meteor.*, **40**, 1485–1499.
- Zawadzki, I. I., 1973: Statistical properties of precipitation patterns. *J. Appl. Meteor.*, **12**, 459–472.
- Zhang, J., and T. Gal-Chen, 1996: Single-Doppler wind retrieval in the moving frame of reference. *J. Atmos. Sci.*, **53**, 2609–2623.
- Ziegler, C., P. S. Ray, and N. C. Knight, 1983: Hail growth in an Oklahoma multicell storm. *J. Atmos. Sci.*, **40**, 1768–1791.